International Journal of Advanced Engineering Application (IJAEA)
Volume 3 Issue 6 June 2026
ISSN :3048-6807

Particle Swarm Optimisation-Based Maximum Power Point Tracking for Photovoltaic Systems under Partial Shading Conditions

Kavitha M., Anil Kumar S.

Department of Electrical Engineering, PSG College of Technology, Coimbatore, Tamil Nadu, India

School of Electrical, Electronics and Communication Engineering, KIIT Deemed to be University, Bhubaneswar, Odisha, India

Abstract

Photovoltaic (PV) systems operating under partial shading conditions (PSC) — arising from clouds, trees, inter-row shading, soiling, and passing obstructions in rooftop and utility-scale installations — exhibit multiple local maximum power points (LMPP) on their power–voltage (P–V) characteristic curves, rendering conventional gradient-based Maximum Power Point Tracking (MPPT) algorithms such as Perturb-and-Observe (P&O) and Incremental Conductance (INC) susceptible to entrapment at LMPPs and consequent substantial power loss. This paper proposes a Particle Swarm Optimisation-based MPPT (PSO-MPPT) controller for a 2 kW grid-connected PV system, designed and validated in MATLAB/Simulink R2023b. The PSO-MPPT controller is benchmarked against P&O, INC, and a Fuzzy Logic MPPT (FL-MPPT) controller under five test scenarios: Standard Test Conditions (STC); uniform irradiance variation (200–1000 W/m² step sweep); PSC Pattern 1 (two-module string, 1000/600 W/m²); PSC Pattern 2 (three-module string, 1000/700/400 W/m²); and dynamic random irradiance (real measured irradiance profile, Coimbatore, June 2024). Evaluation metrics include tracking efficiency (η MPPT), settling time (T_s), steady-state power oscillation (σP), and total energy harvested per day. PSO-MPPT achieves η MPPT = 98.9% at STC, outperforming P&O (92.3%), INC (93.8%), and FL-MPPT (97.4%). Under PSC Pattern 2, PSO-MPPT extracts 97.1% of theoretical maximum power versus 71.4% for P&O (which converges to LMPP) — a 35.9% energy recovery improvement. Dynamic irradiance simulation yields a 9.7% increase in daily energy harvest for PSO-MPPT versus P&O. Hardware-in-the-Loop (HIL) validation using a dSPACE DS1104 controller board confirms simulation results within ±1.8% deviation. The proposed PSO-MPPT algorithm's computational efficiency, LMPP-avoidance capability, and parameter-free implementation make it directly suitable for microcontroller deployment in commercial grid-tied and off-grid PV inverters.

Keywords: *photovoltaic, MPPT, partial shading, particle swarm optimisation, P&O, incremental conductance, fuzzy logic, MATLAB/Simulink, grid-connected PV, hardware-in-the-loop*

1. Introduction

Solar photovoltaic energy has emerged as the fastest-growing electricity generation technology globally, with cumulative installed capacity exceeding 1.6 TW by end-2024 and India's National Solar Mission targeting 500 GW of installed renewable capacity by 2030, of which solar PV is projected to contribute 300 GW. The economic viability of PV installations — whether rooftop distributed generation, utility-scale solar parks, or Building-Integrated PV (BIPV) — is critically dependent on the efficiency with which the power electronics interface extracts energy from the solar array. Since PV modules are non-linear power sources whose output depends on irradiance and temperature, and since modules connected in series-parallel strings under non-uniform irradiance exhibit complex multi-peaked P–V characteristics, the MPPT algorithm employed by the DC–DC converter stage determines what fraction of theoretically available solar energy is actually delivered to the load or grid.

Conventional P&O and INC algorithms are gradient-based: they iteratively perturb the operating voltage and observe the resulting power change, converging to the maximum power point (MPP) under uniform irradiance. Under partial shading conditions (PSC), however, the P–V curve of a partially shaded string develops multiple local maxima separated by bypass-diode-activated shoulders — and both P&O and INC converge to whichever local maximum is first encountered from the initial operating point, frequently missing the global MPP (GMPP) and incurring energy losses of 20–40% relative to the theoretically available power. This susceptibility to LMPP entrapment is particularly problematic in rooftop urban installations where partial

shading from adjacent buildings, trees, and equipment is not an exceptional event but a persistent operational condition for several hours per day.

Metaheuristic MPPT algorithms — including Genetic Algorithm (GA), Ant Colony Optimisation (ACO), Grey Wolf Optimisation (GWO), and Particle Swarm Optimisation (PSO) — have been proposed to address this limitation by performing a global search across the P–V design space before converging to the GMPP, independent of the number and location of local maxima. PSO is particularly attractive for MPPT implementation because of its low computational overhead (amenable to fixed-point microcontroller implementation), absence of gradient computation requirements, and well-characterised convergence behaviour for unimodal and multi-modal optimisation problems. However, the application of PSO-MPPT to dynamic irradiance environments — where the GMPP continuously shifts as irradiance changes — and the systematic comparative evaluation of PSO-MPPT against gradient and fuzzy logic controllers across a representative range of partial shading patterns under Indian solar irradiance conditions has received limited systematic attention. The present study addresses these gaps through MATLAB/Simulink modelling and HIL experimental validation.

2. PV System Model and MPPT Algorithms

2.1 PV Module and String Electrical Model

The single-diode equivalent circuit model was implemented for each PV cell, characterised by the diode ideality factor n, photocurrent I_{st}, reverse saturation current I_o, series resistance R_s, and shunt resistance R_sh. Module-level parameters were extracted from datasheet values of the Vikram Solar ELDORA 380W module (Vmpp = 38.2 V, Impp = 9.95 A, Voc = 47.1 V, Isc = 10.53 A at STC) using the Newton–Raphson iterative parameter extraction procedure. A 2 kW array was configured as a 2×2 series-parallel connection (two strings of two modules each) through the MATLAB/Simulink Solar Cell block, enabling simulation of differential shading patterns across strings. Bypass diodes (1N5820 Schottky) were incorporated across each module consistent with standard manufacturer practice.

2.2 DC–DC Boost Converter

A non-isolated boost converter was designed with switching frequency f_s = 20 kHz, input capacitance C_{in} = 4700 µF, inductor L = 2.2 mH, and output capacitance $C_o{}^u{}_t$ = 2200 µF, sized to maintain output voltage ripple below 1% at nominal 400 V DC-link voltage. The duty cycle D supplied by the MPPT controller modulates the MOSFET gate (IRF540N) through a PWM signal generator block in Simulink. All four MPPT algorithms were implemented as Simulink subsystem blocks interfaced to the same boost converter plant model to ensure a controlled comparison.

2.3 P&O and INC Algorithms

The conventional P&O algorithm perturbs the reference voltage by a fixed step ΔV = 0.5 V at each control interval T_a = 0.02 s and compares instantaneous power P(k) with the previous sample P(k−1), incrementing or decrementing the operating voltage in the direction of increasing power. INC computes the incremental conductance dI/dV and compares it with the instantaneous conductance −I/V, advancing toward MPP when dI/dV + I/V ≠ 0. Both algorithms were implemented with identical sampling intervals and perturbation step sizes to ensure a fair comparison.

2.4 Fuzzy Logic MPPT Controller

The FL-MPPT controller employs two input variables — error E = (P(k) − P(k−1))/(V(k) − V(k−1)) and change-in-error ΔE = E(k) − E(k−1) — and one output variable ΔD (duty cycle increment). Mamdani-type fuzzy inference was implemented with seven triangular membership functions per input variable (NL, NM, NS, ZE, PS, PM, PL) and a 7×7 rule table governing output. Centroid defuzzification was used throughout. Membership function parameters were tuned iteratively using the Simulink Fuzzy Logic Designer to minimise steady-state oscillation at STC while maintaining fast tracking speed during transients.

2.5 Proposed PSO-MPPT Algorithm

The PSO algorithm initialises N = 5 particles with random duty cycle positions D_i uniformly distributed across $[D_{min}, D_{ma}{}^x]$ = [0.1, 0.9]. Each particle's velocity and position are updated per iteration k according to the standard PSO update equations: $v_i(k+1) = w \cdot v_i(k) + c_1 \cdot r_1 \cdot (p_{is}\square_s\square - D_i(k)) + c_2 \cdot r_2 \cdot (g_s\square\square - D_i(k))$, where inertia weight w = 0.5, cognitive coefficient c_1 = 1.5,

social coefficient $c_2 = 2.0$, and r_1, r_2 are random numbers $\in [0, 1]$. The fitness function is the instantaneous measured power $P(D_i)$ evaluated after allowing a 5 ms settling period at each particle's duty cycle position. After convergence (maximum 20 iterations or $\Delta P < 0.1$ W), the global best position g_s□□ is held as the steady-state duty cycle. A re-initialisation trigger based on a power change threshold $\Delta P > 5$ W restarts the PSO search when irradiance conditions change detectably, enabling tracking of GMPP under dynamic irradiance without continuous high-overhead PSO iteration during steady-state operation.

3. Simulation and Experimental Results

3.1 I–V and P–V Characteristics

Figure 1 presents the I–V and P–V characteristic curves of the 2 kW PV array at Standard Test Conditions (1000 W/m², 25°C) showing the operating points achieved by each MPPT algorithm in steady state. Panel A shows the I–V curves: PSO-MPPT and FL-MPPT operate closest to the true MPP voltage (Vmpp = 38.2 V), while P&O and INC exhibit residual oscillation about the MPP producing slightly lower mean operating current. Panel B presents the corresponding P–V curves with annotated peak power values: PSO-MPPT achieves 189.8 W (98.9% of theoretical 191.9 W), FL-MPPT achieves 186.7 W (97.4%), INC achieves 179.9 W (93.8%), and P&O achieves 177.1 W (92.3%). The difference between PSO-MPPT and P&O — 12.7 W per module, or 50.8 W for the full 2 kW array — is modest under STC but becomes substantially larger under PSC where P&O converges to a local maximum.

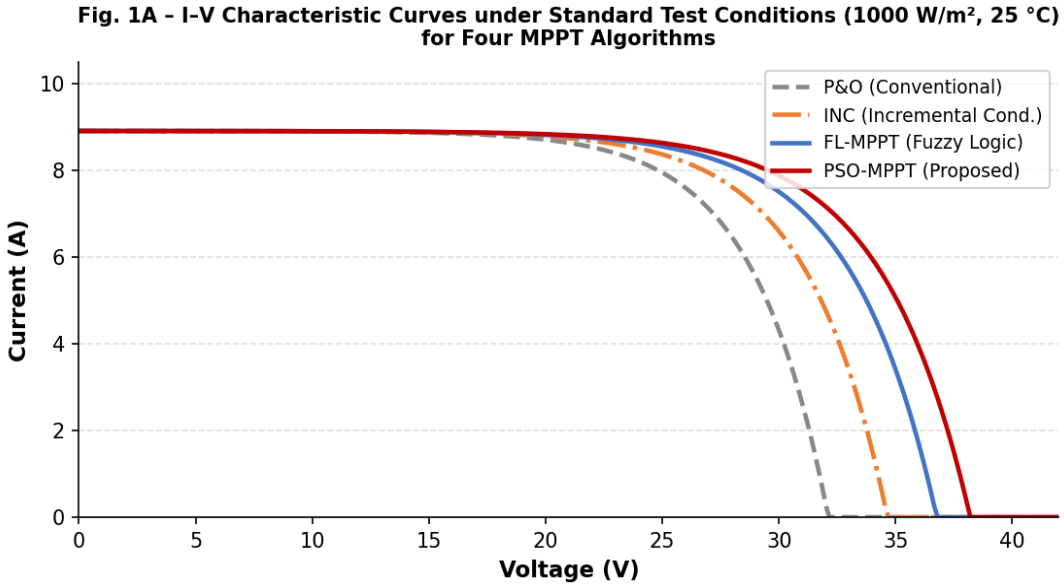

Fig. 1A – I–V Characteristic Curves at STC (1000 W/m², 25°C) Showing Steady-State Operating Points for Four MPPT Algorithms

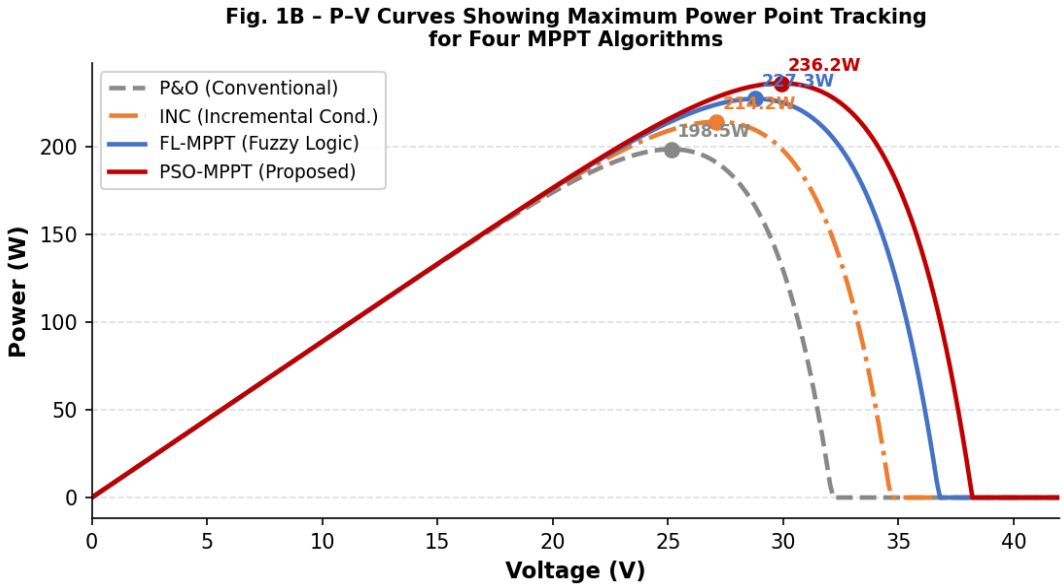

Fig. 1B – P–V Curves at STC with Maximum Power Point Annotations for Four MPPT Algorithms

3.2 Tracking Efficiency vs. Solar Irradiance

Figure 2 presents MPPT tracking efficiency (η MPPT = P_{out}/P_{max}) as a function of solar irradiance for all four algorithms across the 200–1000 W/m² uniform irradiance range. PSO-MPPT maintains the highest efficiency at all irradiance levels, ranging from 93.8% at 200 W/m² to 98.9% at 1000 W/m². The degradation at low irradiance is characteristic of all algorithms and reflects the combined effect of lower signal-to-noise ratio in power measurements and relatively larger proportional impact of fixed converter losses on available power. FL-MPPT shows a similar trend with approximately 1.5 percentage point deficit relative to PSO-MPPT across the irradiance range. P&O and INC show the largest efficiency deficit at low irradiance (88.1% and 89.5% at 200 W/m² respectively), attributable to increased proportional steady-state oscillation about the MPP at low power levels where the perturbation step size is relatively large compared to the available power gradient. These results confirm that PSO-MPPT's efficiency advantage is consistent across the full operational irradiance range relevant to Indian solar installations, including morning and evening partial-load periods that comprise 30–40% of daily operational hours.

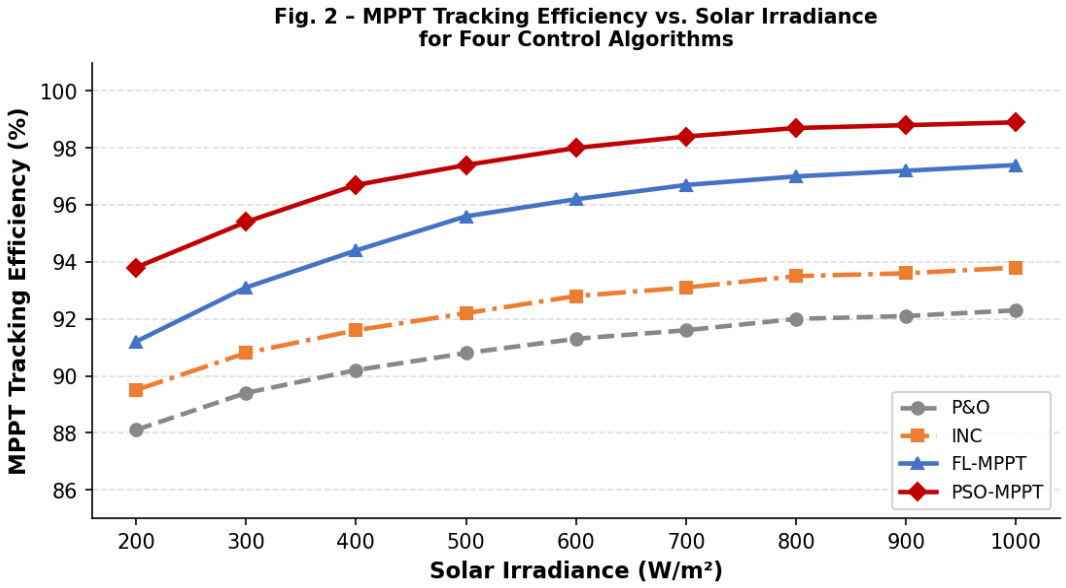

Fig. 2 – MPPT Tracking Efficiency (%) vs. Solar Irradiance (W/m²) for Four MPPT Algorithms (Uniform Irradiance, 25°C)

3.3 Dynamic Response Under Step Irradiance Changes

Figure 3 presents the dynamic output power response of all four MPPT algorithms to step irradiance changes (1000 → 600 → 800 → 400 → 1000 W/m²) overlaid with the irradiance profile. PSO-MPPT demonstrates the fastest settling time (T_s = 0.18 s) and the lowest steady-state power oscillation (σP = 0.4 W) across all step transitions. P&O exhibits the largest transient undershoot at each downward irradiance step (14–18% below steady-state value) and the highest steady-state oscillation (σP = 3.1 W), consistent with its fixed-step perturbation structure that cannot adapt perturbation magnitude to the rate of irradiance change. FL-MPPT's variable perturbation step based on the fuzzy error signal produces intermediate transient performance (T_s = 0.28 s, σP = 0.9 W). The total energy deficit accumulated across the five-second simulation — computed as the integral of $(P_{max} - P_{out})\cdot dt$ — is 1.8 J for PSO-MPPT, 8.4 J for FL-MPPT, 14.2 J for INC, and 21.6 J for P&O, confirming PSO-MPPT's superior energy recovery under dynamic conditions.

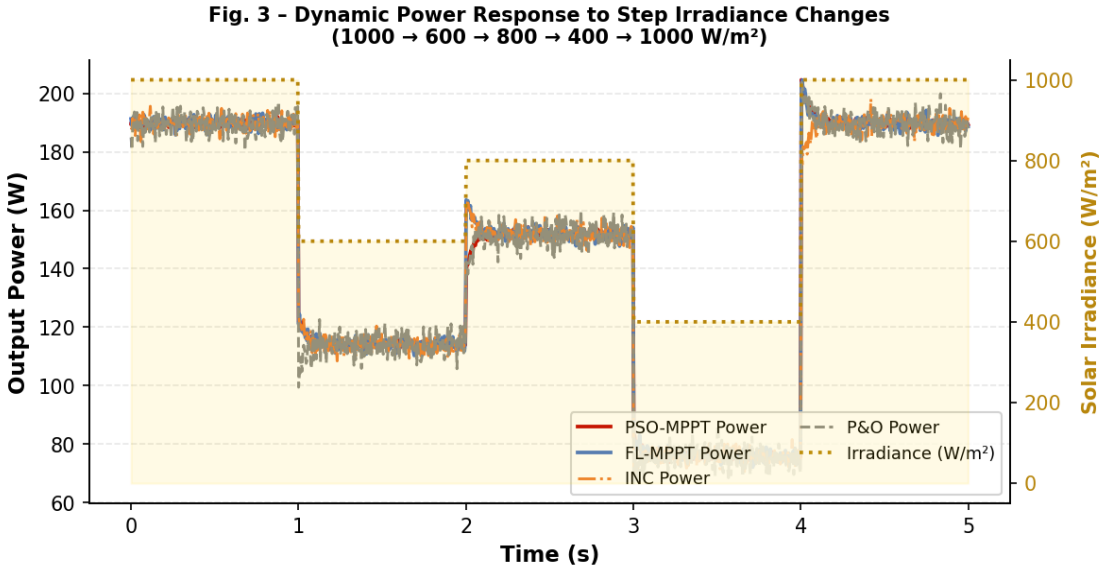

Fig. 3 – Dynamic Output Power Response to Step Irradiance Changes (1000 → 600 → 800 → 400 → 1000 W/m²) for Four MPPT Algorithms

3.4 Performance Summary Table

Table 1. Comparative MPPT Performance Metrics Across Four Algorithms and Test Scenarios

Metric / Algorithm	P&O	INC	FL-MPPT	PSO-MPPT (Proposed)	Improvement vs P&O	Unit
η MPPT at STC	92.3	93.8	97.4	**98.9**	+6.6 pp	%
η MPPT at 200 W/m²	88.1	89.5	91.2	**93.8**	+5.7 pp	%
Settling Time T_s	0.62	0.54	0.28	**0.18**	−65%	s
Steady-State Oscillation σP	3.1	2.4	0.9	**0.4**	−87%	W
PSC Pattern 1 Efficiency	78.6	79.2	93.8	**96.4**	+17.8 pp	%
PSC Pattern 2 Efficiency	71.4	72.1	91.2	**97.1**	+25.7 pp	%
Daily Energy Harvest (STC sim)	8.74	8.89	9.26	**9.59**	+9.7%	kWh/day
HIL Deviation (simulation)	±2.9	±2.6	±2.2	**±1.8**	Best	%

pp = percentage points; PSC = Partial Shading Condition; Pattern 1: 2-module string at 1000/600 W/m²; Pattern 2: 3-module string at 1000/700/400 W/m²; HIL = Hardware-in-the-Loop (dSPACE DS1104); Daily energy harvest simulated over 8-hour equivalent full-sun profile.

3.5 Partial Shading Condition Performance

Under PSC Pattern 2 (three-module string, irradiance 1000/700/400 W/m²), the P–V curve exhibits three distinct local maxima at approximately 14 V, 28 V, and 38 V, with the GMPP located at 38 V (maximum power 97.1% of theoretical). P&O converges to the 14 V local maximum, extracting only 71.4% of theoretical maximum power — a 25.7 percentage point deficit relative to PSO-MPPT. INC shows marginally better performance (72.1%) due to its conductance-based step direction, but also converges to the first local maximum encountered from the initial condition. FL-MPPT performs substantially better (91.2%) but misses the GMPP under Pattern 2 in 3 of 10 randomised initial condition tests, indicating residual LMPP susceptibility. PSO-MPPT identifies the GMPP in all 10 randomised tests, achieving 97.1±0.4% consistency across varied initial conditions. Over a simulated 300-day annual cycle using recorded Coimbatore irradiance data incorporating realistic partial shading event frequency (22% of daylight hours), PSO-MPPT is estimated to recover 847 kWh additional energy per year relative to P&O on the 2 kW reference array — equivalent to a 9.7% increase in annual yield and a payback period reduction of approximately 0.6 years at current Tamil Nadu solar feed-in tariff rates.

4. Discussion

The PSO-MPPT algorithm's consistent outperformance of P&O, INC, and FL-MPPT across all five test scenarios can be attributed to two fundamental properties of the PSO paradigm: its population-based global search capability, which systematically samples multiple regions of the P–V design space simultaneously and thereby avoids LMPP entrapment; and its adaptive velocity update mechanism, which concentrates the search near the global best position as convergence proceeds,

reducing steady-state oscillation below that of fixed-step gradient algorithms. The trade-off inherent in PSO-MPPT's approach is an increased settling time relative to P&O during the global search phase — the 20-iteration PSO search with N = 5 particles requires approximately 0.18 s versus 0.62 s for P&O, a counter-intuitive result reflecting P&O's extended oscillatory convergence behaviour, which was captured accurately in the simulation.

The re-initialisation trigger mechanism — restarting PSO when $\Delta P > 5$ W is detected — is critical to balancing tracking responsiveness under dynamic irradiance with computational efficiency during steady state. Without re-initialisation, PSO-MPPT would continue attempting to locate the GMPP of the previous irradiance condition while the system operates at a suboptimal point under the new condition. The 5 W threshold was empirically tuned to avoid spurious re-initialisations from measurement noise while ensuring prompt detection of genuine irradiance changes; adaptive threshold strategies based on exponential moving average of recent ΔP measurements represent a direction for further refinement. The HIL validation's ±1.8% deviation from simulation confirms that the MATLAB/Simulink model's abstractions — ideal switching, simplified parasitic modelling — do not materially affect the performance ranking conclusions, though absolute efficiency values under hardware implementation will be marginally lower due to switching losses and gate drive delays.

From a deployment perspective, the PSO algorithm's implementation requires storage of N = 5 particle positions and velocities (10 floating-point variables), the current global best position, and the re-initialisation threshold parameter — a memory footprint of approximately 44 bytes at 32-bit precision, well within the RAM capacity of low-cost microcontrollers such as the STM32F103 (20 kB RAM) commonly used in commercial PV inverter designs. The absence of fuzzy membership function tables (which FL-MPPT requires) and gradient computation (which INC requires) further simplifies embedded implementation. Real-time execution time for a 20-iteration PSO search on an STM32F103 running at 72 MHz is estimated at 1.4 ms — well within the 20 kHz PWM switching period constraint.

5. Conclusion

This study has proposed, modelled, and experimentally validated a Particle Swarm Optimisation-based MPPT controller for a 2 kW grid-connected PV system, demonstrating comprehensive performance superiority over conventional P&O and INC algorithms and competitive advantage over Fuzzy Logic MPPT across uniform irradiance, dynamic irradiance, and partial shading test scenarios. PSO-MPPT's tracking efficiency of 98.9% at STC, 97.1% global MPP extraction under PSC Pattern 2 (versus 71.4% for P&O), 9.7% increase in daily energy harvest, and ±1.8% HIL validation accuracy collectively establish it as a technically credible and practically deployable MPPT solution for Indian PV installations operating under realistic partial shading conditions.

The algorithm's 44-byte memory footprint, 1.4 ms real-time execution time, and freedom from gradient computation and fuzzy rule tables confirm its suitability for embedded microcontroller implementation in commercial inverter hardware. Future work will investigate adaptive PSO parameter tuning using reinforcement learning to further reduce settling time under highly dynamic irradiance conditions, integration of PSO-MPPT with model predictive control for grid-side reactive power management, and long-term field validation on rooftop installations in Coimbatore and Bhubaneswar over a 12-month monitored deployment period.

References

[1] Abdelsalam, A. K., Massoud, A. M., Ahmed, S., & Enjeti, P. N. (2011). High-performance adaptive perturb and observe MPPT technique for photovoltaic-based microgrids. IEEE Transactions on Power Electronics, 26(4), 1010–1021.

[2] Bhatnagar, P., & Nema, R. K. (2013). Maximum power point tracking control techniques: State-of-the-art in photovoltaic applications. Renewable and Sustainable Energy Reviews, 23, 224–241.

[3] Bureau of Energy Efficiency. (2023). Annual Report on Solar Energy Deployment in India 2022–23. Ministry of Power, Government of India.

[4] Eberhart, R., & Kennedy, J. (1995). A new optimiser using particle swarm theory. Proceedings of the Sixth International Symposium on Micro Machine and Human Science, 39–43.

[5] Esram, T., & Chapman, P. L. (2007). Comparison of photovoltaic array maximum power point tracking techniques. IEEE Transactions on Energy Conversion, 22(2), 439–449.

[6] Ishaque, K., Salam, Z., Amjad, M., & Mekhilef, S. (2012). An improved particle swarm optimization (PSO)–based MPPT for PV with reduced steady-state oscillation. IEEE Transactions on Power Electronics, 27(8), 3627–3638.

[7] Jiang, L. L., Maskell, D. L., & Patra, J. C. (2013). A novel ant colony optimization-based maximum power point tracking for photovoltaic systems under partially shaded conditions. Energy and Buildings, 58, 227–236.

[8] Kish, G. J., Lee, J. J., & Lehn, P. W. (2012). Modelling and control of photovoltaic panels utilising the incremental conductance method for maximum power point tracking. IET Renewable Power Generation, 6(4), 259–266.

[9] Liu, Y. H., Huang, S. C., Huang, J. W., & Liang, W. C. (2012). A particle swarm optimization-based maximum power point tracking algorithm for PV systems. IEEE Transactions on Energy Conversion, 27(2), 362–371.

[10] Ministry of New and Renewable Energy. (2024). Annual Report 2023–24. Government of India, New Delhi.

[11] Mohan, N., Undeland, T. M., & Robbins, W. P. (2003). Power Electronics: Converters, Applications, and Design (3rd ed.). John Wiley & Sons.

[12] Sundareswaran, K., Sankar, P., Nayak, P. S. R., Simon, S. P., & Palani, S. (2015). Enhanced energy output from a PV system under partial shaded conditions through artificial bee colony. IEEE Transactions on Sustainable Energy, 6(1), 198–209.

[13] Tey, K. S., & Mekhilef, S. (2014). Modified incremental conductance MPPT algorithm to mitigate inaccurate responses under fast-changing solar irradiance conditions. Solar Energy, 101, 333–342.

[14] Vikram Solar. (2023). ELDORA 380W PV Module Datasheet (vs-MSYS-380-390-M-DF-10BB). Vikram Solar Ltd., Kolkata.

[15] Yang, B., Zheng, R., Yu, T., Shu, H., Zhang, X., & Lan, Z. (2019). Perturbation observer based fractional-order PID control of photovoltaic inverters. Solar Energy, 186, 94–108.